Geophysical Research Letters

RESEARCH LETTER
10.1029/2025GL115772

Differences in Regional Home Heating Behavior in Three U.S. Cities Revealed by Ground-Based Sensor Network

Naomi G. Asimow[1], Milan Y. Patel[2], Yishu Zhu[1], Anna R. Winter[2], Kevin R. Gurney[3], William M. Berelson[4], Alexander J. Turner[1], and Ronald C. Cohen[1,2]

[1]Department of Earth and Planetary Science, University of California, Berkeley, CA, USA, [2]College of Chemistry, University of California, Berkeley, CA, USA, [3]School of Informatics, Computing, and Cyber Systems, Northern Arizona University, Flagstaff, AZ, USA, [4]Department of Earth Sciences, University of Southern California, Los Angeles, CA, USA

Key Points:

- Observations from a dense CO_2 sensor network coupled with Bayesian inversions are shown to be sensitive to urban home heating emissions
- Critical temperatures for home heating vary regionally: Bay Area (16.5°C), Los Angeles (18.5°C), and Houston (18.8°C)
- The method is sufficiently sensitive to reproduce the critical temperature and seasonality of home heating, even when withheld from priors

Supporting Information:

Supporting Information may be found in the online version of this article.

Correspondence to:

R. C. Cohen,
rccohen@berkeley.edu

Citation:

Asimow, N. G., Patel, M. Y., Zhu, Y., Winter, A. R., Gurney, K. R., Berelson, W. M., et al. (2025). Differences in regional home heating behavior in three U.S. Cities revealed by ground-based sensor network. *Geophysical Research Letters*, *52*, e2025GL115772. https://doi.org/10.1029/2025GL115772

Received 6 MAR 2025
Accepted 23 JUN 2025

Abstract Home heating preferences vary dramatically with regional climate. The temperature at which residents turn on natural gas home heating systems (critical temperature) varies by as much as 25°C from the northern to southern United States (U.S.). Here we derive temperature dependent CO_2 emissions in three U.S. cities using a dense ground-based CO_2 observation network. A Bayesian inverse modeling methodology is used to update a 1-km emission inventory in each of the three cities. This method is able to correctly identify the critical temperature of home heating even when this information is withheld from the prior inventory, as verified by natural gas distribution data. Variance in regional heating practices has not been previously demonstrated with ground-based networks of CO_2 observations. This result provides evidence that a Bayesian inverse modeling framework is sensitive to emissions of the home heating sector.

Plain Language Summary This work uses measurements of atmospheric CO_2 to determine the temperature at which people turn on their heat in the Bay Area, Los Angeles, and Houston. Previous studies have used natural gas distribution data to show that this temperature varies with regional climate. This study is the first to show that a network of CO_2 sensors and an atmospheric model can detect this effect.

1. Introduction

Buildings are responsible for 31% of global CO_2 emissions (IPCC, 2023a) and building heating accounts for a large fraction of building emissions. The International Energy Agency found heating-related CO_2 emissions of 5.0 $GtCO_2$ in 2019 (IEA, 2021), 11% of the global total CO_2 emissions that year (IPCC, 2023b). In colder regions of the world, building heating is responsible for an even larger fraction of emissions (IPCC, 2023a).

In the United States (U.S.), 64% of heated households are heated using combustible fuel, primarily natural gas (EIA, 2017). Addressing the emissions from space heating of buildings is important for achieving climate goals, both because of CO_2 emitted during combustion and the large contribution of gas infrastructure pipeline leaks to global methane emissions (Brandt et al., 2014). Replacing natural gas heating systems with electric heat pumps has the potential to save significant CO_2 emissions, with savings dependent on the fuel-mix of the electricity grid and the efficiency of the gas appliance being replaced (Walker et al., 2022). The transition to heat pumps has been relatively slow in the U.S., with 0.2% of households claiming a tax credit for heat pump adoption in 2023 (IRS, 2023).

Natural gas usage varies by household due to behavioral factors and home characteristics (Verhallen & Raaij, 1981). Household natural gas demand is also affected by energy prices and household income (Alberini et al., 2011). Mittakola et al. show that household gas demand is flat with respect to temperature above a certain critical temperature (T_{crit}). Below T_{crit}, it is cold enough that home heating systems are powered on, and gas demand shows a linear increase with decreasing temperature. Using natural gas distribution data from 1000 U.S. counties, the authors find a median T_{crit} of 16.5°C with tremendous regional variation. In some counties in the northern U.S., T_{crit} is as low as 0°C, while in certain southern U.S. counties T_{crit} exceeds 25°C.

Both activity-based and atmospheric-based methods have been used to quantify heating CO_2 emissions at sub-city scales. Fuel consumption data sets provide a strong activity-based constraint on regional home heating behavior (Mittakola et al., 2024) and approximately 100% of home heating fuel combusted is fully oxidized to CO_2 (IPCC, 2006). However, developing fine-scale inventories (i.e., 1 km, hourly) from fuel consumption statistics can be challenging due to the lack of public fuel consumption data sets at sufficiently fine spatial and temporal

scales. Atmospheric-based Bayesian inversion methods can provide additional constraints on activity-based inventories, but most atmospheric-based strategies rely on post-processing steps (often including additional data sets) to separate the contribution of heating emissions from other sectors (Asimow et al., 2024; Lian et al., 2023; Turner et al., 2020). Further, atmospheric-based methods are subject to additional uncertainties resulting from measurement uncertainty, transport model error, representation error, error in the background concentration, and uncertainty in biospheric fluxes (Feng et al., 2019; Lian et al., 2023; Martin et al., 2019; Munassar et al., 2023). Given the strong activity-based constraints on differing regional home heating behavior, withholding this information from a prior inventory and solving for emissions provides a valuable sensitivity test of the Bayesian inversion system. Is the inversion system sufficiently sensitive to regional home heating emissions to differentiate the temperature at which home heating systems are powered on in different cities?

Previously, our group demonstrated the use of a ground-based sensor network, the Berkeley Environmental Air Quality and CO_2 Network ($BEACO_2N$), for constraining emissions at sub-city scales within the San Francisco (SF) Bay Area, California (Asimow et al., 2024; Turner et al., 2020). The network measures CO_2, CO, NO, NO_2, O_3, and aerosol particles in the SF Bay Area with approximately 2-km spacing and has been deployed since 2018 in the present configuration (Delaria et al., 2021; Shusterman et al., 2016; Winter et al., 2025). With collaborators, similar ongoing $BEACO_2N$ networks have been deployed in Glasgow, Scotland (deployed 2020, part of The Glasgow Environmental Monitoring of Indoor and Outdoor Air project), Los Angeles, California (deployed 2021, also called Carbon Census), and Providence, Rhode Island (deployed 2022, also called Breathe Providence) (Breathe Providence, n.d.; GEMINOA, n.d.; Kim et al., 2025). Temporary deployments also occurred in New York City, New York (2018–2019), and Houston, Texas (2018–2021).

Here, an inversion methodology developed for the SF Bay Area is applied to two additional U.S. cities. The three cities have distinct climates (Palecki et al., 2020). San Francisco has a mild climate year-round (winter minimum 8.1°C, summer maximum 21.2°C), Los Angeles has mild winters and warmer summers (9.0°, 28.9°C), and Houston has mild winters with the hottest summers (6.5°, 34.9°C). While the three cities share similar emission sectors with traffic as the largest source, residential emissions dominate more in the Bay Area, industrial emissions are prominent in Los Angeles, and electricity production contributes more in Houston (Figure S5 in Supporting Information S1).

We conduct 1 year of inversions in both Los Angeles and Houston and 4.5 years of inversions in the SF Bay Area. In each city, any information regarding temperature dependence of emissions is withheld from the prior inventory. A comparison of the posterior emissions of the three urban regions yields differences in the temperature dependence of emissions in agreement with known natural gas distribution data. This result demonstrates the inversion system's ability to detect temperature-dependent patterns in urban CO_2 emissions that are consistent with expected regional home heating behaviors, suggesting this approach can help distinguish the seasonal contribution of home heating to overall urban emissions.

2. Methods

We conducted inversions in three urban regions of the U.S. Results for the SF Bay Area have been previously published (Asimow et al., 2024). In this work, we extend the inversion methodology from the SF Bay Area to Los Angeles and Houston and analyze the temperature dependence of the emissions in these three urban areas.

2.1. Observing System

Ambient CO_2 was measured every 4 s using the Vaisala CARBOCAP Carbon Dioxide Probe GMP343 in the three urban regions of the study: regions of the SF Bay Area, Los Angeles, and Houston. The data were averaged to hourly resolution for this analysis. Figure 1 shows measurement site locations. During the study period, 59 sensors were active in the Bay Area, 16 sensors were active in Houston, and 11 sensors were active in Los Angeles. Details on the instrument and network design are available in previous publications (Delaria et al., 2021; Shusterman et al., 2016). Network spacing is similar in the Bay Area and Houston and sparser in Los Angeles. The mean distance from each sensor node to its nearest node was 1.7 km (σ = 0.6 km) in the Bay Area, 2.5 km (σ = 0.9 km) in Los Angeles, and 1.8 km (σ = 0.7 km) in Houston.

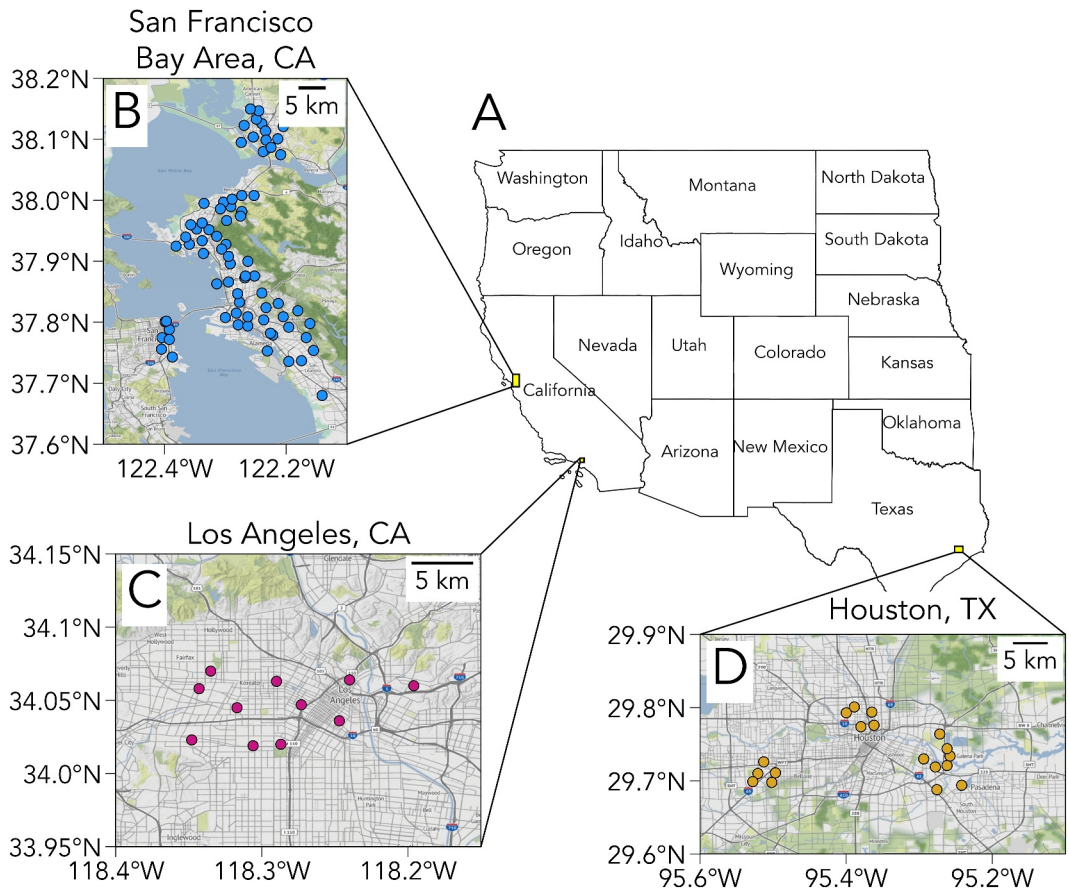

Figure 1. Map of the Berkeley Environmental Air Quality and CO_2 Network sensor coverage during the study period in three urban regions (b–d) shown as insets on a map of the western United States (a). Background map credits: © Stadia Maps (stadiamaps.com), © Stamen Design (stamen.com), © OpenMapTiles (openmaptiles.org), © OpenStreetMap (openstreetmap.org/copyright).

2.2. Prior Anthropogenic CO_2 Emission Inventories

The Bay Area prior used was developed by our group and is a 1-km, hourly inventory. This inventory includes vehicle emissions (from the National Oceanic and Atmospheric Administration Fuel-based Inventory of Vehicle Emission), and large point source emissions and county-level natural gas emissions reported by the Bay Area Air Quality Management District (Mangat et al., 2010; McDonald et al., 2014; Turner et al., 2016, 2020). This inventory has diurnal and day-of-week variation, but no seasonal variation.

The Vulcan Version 3.0 inventory from the most recently available model year (2015) was used for both Los Angeles and Houston (Gurney et al., 2020). Unlike the Bay Area inventory, Vulcan includes seasonal heating variation. In order to withhold prior information on home heating behavior for the analysis, we utilize seasonally averaged Vulcan emissions in our priors. Seasonally averaged emissions in each grid cell are calculated by taking the temporal mean for each hour of the week across 1 year of Vulcan data. The resulting gridded anthropogenic emissions used in the prior have diurnal and day-of-week variation, but no seasonal variation.

2.3. Biospheric Emissions

To create a 1-km and hourly estimate of biospheric fluxes, we use a gross primary productivity (GPP) product that is based on measurements of solar-induced chlorophyll fluorescence (SIF) from the TROPOspheric Monitoring Instrument (TROPOMI) (Turner et al., 2021, 2022). From this daily product for plant uptake of CO_2, we assume an annual GPP to respiration scaling of 0.822 (Baldocchi & Penuelas, 2019), which is shown to be applicable over a range of ecosystems. GPP is partitioned over the course of the day, scaled according to the cosine of the solar zenith

angle. Respiration is partitioned annually using seasonal temperature and partitioned diurnally following Yang et al., 2014.

2.4. Inversion System

The Stochastic Time-Inverted Lagrangian Transport Model (STILT) was used to compute a surface influence for each hourly $BEACO_2N$ observation at each measurement site (Fasoli et al., 2018; Lin et al., 2003). Meteorology was obtained from NOAA's High Resolution Rapid Refresh (HRRR) product (Benjamin et al., 2016). We invert for hourly CO_2 fluxes at 1-km following Equation 1:

$$\hat{\mathbf{x}} = \mathbf{x_a} + (\mathbf{HB})^{\mathbf{T}}\left(\mathbf{HBH^T} + \mathbf{R}\right)^{-1}(\mathbf{y} - \mathbf{Hx_a}) \quad (1)$$

where $\mathbf{x_a}$ is the prior, $\mathbf{H}$ is the HRRR-STILT footprints, $\mathbf{B}$ is the prior error covariance matrix, $\mathbf{R}$ is the model-data mismatch error covariance matrix, $\mathbf{y}$ is the $BEACO_2N$ measurements, and $\hat{\mathbf{x}}$ is the posterior fluxes at 1-km x 1-km resolution. The inversion methodology is described in detail in Text S1, as well as in previous publications (Asimow et al., 2024; Turner et al., 2020). The prior error covariance matrix, $\mathbf{B}$, is formulated as a Kronecker product of a spatial prior error covariance matrix and a temporal prior error covariance matrix (Yadav & Michalak, 2013). Upwind, or background, CO_2 is a major source of uncertainty in inversions. As such, we do not treat the upwind concentration as a known value, but instead formulate the prior with an estimate of upwind concentration at the domain edges, which is able to be updated along with the fluxes. The prior upwind concentration is taken from OCO-2 Goddard Earth Observing System (GEOS) L3 assimilated data set at the lowest model level (Weir et al., 2021). We solve Equation 1 to generate posterior fluxes once for each day in each region using 96-hr overlapping windows.

We solve for hourly emissions over 4.5 years in the Bay Area (January 2018–July 2022) and 1 year each in Houston (March 2020–February 2021) and Los Angeles (July 2021–July 2022). We remove the prior biospheric fluxes (TROPOMI-SIF) and crop the fluxes to the 40th percentile contour of surface influence (region of influence), as described in Asimow et al., 2024. The region of influence determination for each city is shown in Figure S1 in Supporting Information S1. Per capita emissions within the region of influence are calculated using a 1-km population density map (Figure S3 in Supporting Information S1) (WorldPop & Bondarenko, 2020).

While the posterior error covariance matrix is often used to characterize the uncertainty in Bayesian inversions, computation of this matrix was computationally intractable. We instead estimate the uncertainty of the posterior using the 1σ spread of the posterior estimates over 6 weeks averaging time. Spatial uncertainties are explored further in Figure S10 in Supporting Information S1. The improved agreement of the simulated concentrations with the observed CO_2 concentrations using the posterior fluxes is shown in Figure S11 in Supporting Information S1.

2.5. Temperature Dependence Analysis

Historical daily mean temperatures for Oakland, Los Angeles, and Houston were obtained from visualcrossing.com (Visual Crossing, n.d.). Outlier days >2 standard deviations from the mean (in temperature or emissions) are discarded for each of the three cities. Daily mean temperatures are split into 30 quantile bins for each city and the median emission between the hours of 0:00 and 6:00 local time for each city is found for each temperature quantile bin. Posterior emissions were limited to early morning hours to maximize the signal of the residential emission sector relative to the other sources. The hours of 0:00–6:00 were chosen based on the mean diurnal pattern of fractional contributions of the 10 emission sectors in Vulcan within the influence region of each city (Figure S5 in Supporting Information S1). We plot the median early morning emissions versus temperature quantile. We define a custom piecewise fitting function (Equation 2) and fit the coefficients of the function using the LMFIT package to determine T_{crit}, m, and b with uncertainties (Newville et al., 2024). Temperature bins >25°C are excluded from the fitting due to the likelihood of emissions from electricity demand for home cooling in Houston (discussed in detail in Section 3.2 and shown in Figure S8 in Supporting Information S1). We test the sensitivity of the derived T_{crit} to the 25°C assumption in Figure S12 in Supporting Information S1.

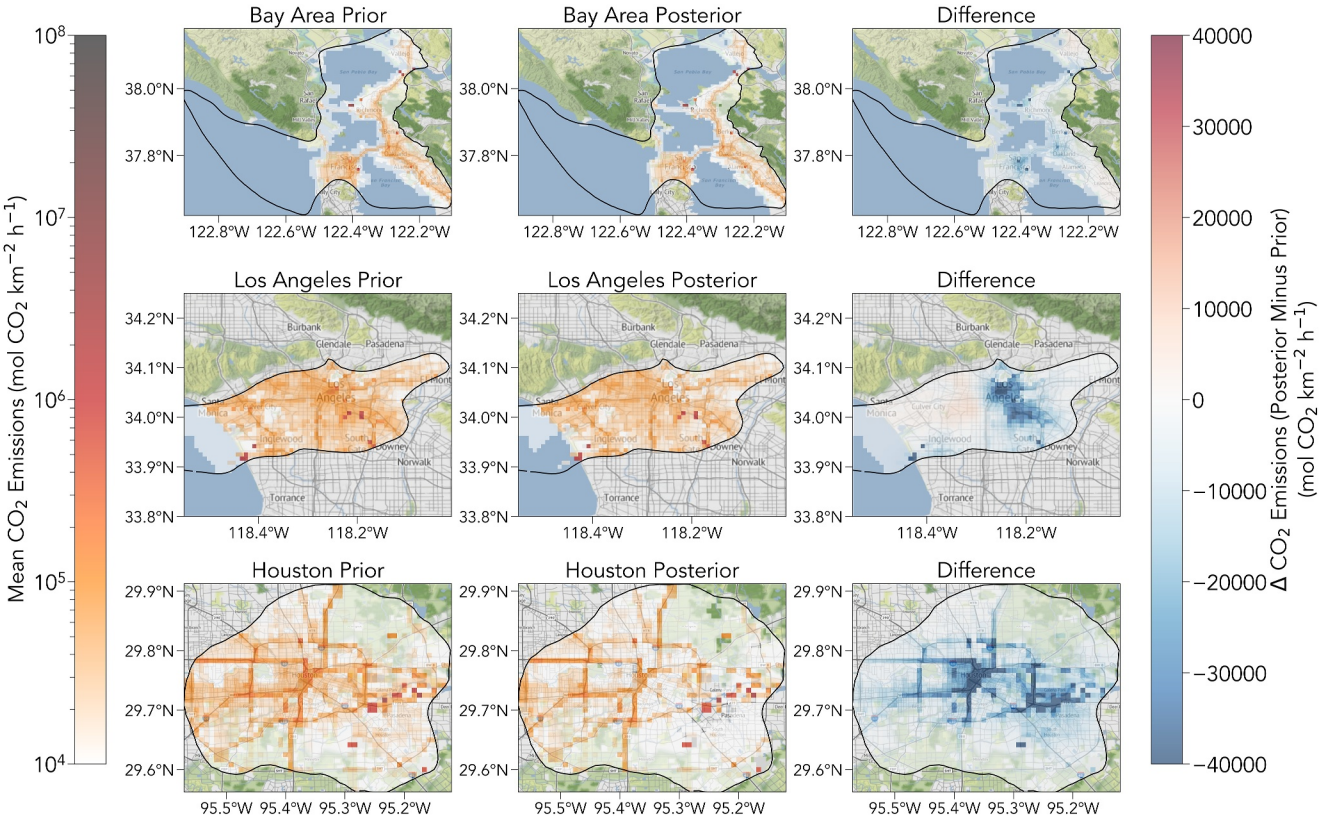

Figure 2. Spatial patterns of the prior, posterior, and difference in anthropogenic emissions for each of the 3 cities. Note that prior and posterior emissions are shown on a log scale, while differences are presented on a linear scale. Emissions shown are averaged over all times of day and the entire study period. The black trace represents the region of influence (40th percentile contour of cumulative footprint influence). Background map credits: © Stadia Maps (stadiamaps.com), © Stamen Design (stamen.com), © OpenMapTiles (openmaptiles.org), © OpenStreetMap (openstreetmap.org/copyright).

$$\mathbf{f(T)} = \begin{cases} \boldsymbol{b} + \boldsymbol{m}\,(\boldsymbol{T} - \boldsymbol{T}_{\mathbf{crit}}) & \textit{if} \quad \boldsymbol{T} < \boldsymbol{T}_{crit} \\ \boldsymbol{b} & \textit{if} \quad \boldsymbol{T} \geq \boldsymbol{T}_{crit} \end{cases} \tag{2}$$

3. Results and Discussion

3.1. Posterior Emissions

Prior and posterior anthropogenic emissions for each of the three cities are shown in Figure 2. Posterior emissions decreased (compared to the prior) in all three cities, with largest changes in Houston. Mean Bay Area emissions decreased by 15.1%, Los Angeles by 13.3%, and Houston by 25.4% from the prior to the posterior. Decreases in the SF Bay Area appear most strongly at distinct large point sources, such as the Chevron refinery in Richmond, California, as well as along highways. In Los Angeles, posterior emissions were most decreased in the downtown area and showed slight increases in the western area of the region of influence. In Houston, decreases largely follow the highways. The spatial pattern of the differences shown in Figure 2 largely resembles the magnitude of the emissions in the prior, since the diagonals of the spatial component of the prior error covariance matrix, **B**, incorporate a 50% error on the prior emissions. However, spatial patterns in the difference are also influenced by the magnitude of the footprints in **H** and the magnitude of the mismatch between modeled concentrations and observed concentrations ($\mathbf{y}$-$\mathbf{Hx_a}$). A two-sided paired *t*-test is employed to determine which locations have statistically significant changes from the mean prior emissions to mean posterior emissions (Figure S10 in Supporting Information S1).

A timeseries of prior and posterior emissions (6-week rolling means) for each city is given in Figure 3. In Asimow et al., 2024, we showed that the posterior flux uncertainty over the influence region is decreased by ~25% when

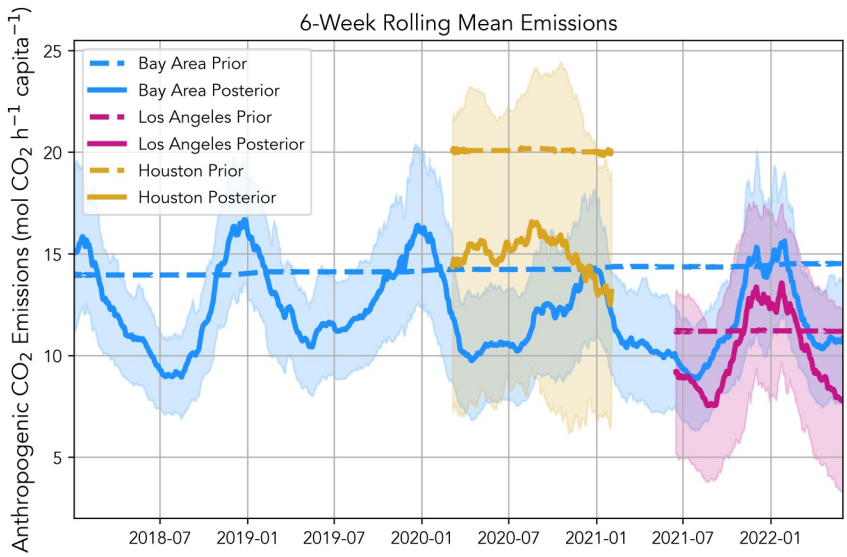

Figure 3. Timeseries of prior and posterior per capita anthropogenic CO_2 emissions for each of the cities studied. Each timeseries is a rolling 6-week mean. The shaded region represents the rolling 1σ range on the posterior emissions.

averaged over 6 weeks. Since each city has a different area within its region of influence with differing fractions of water area, the total emissions (and the per area emissions) of the three regions are not directly comparable. We present per capita emissions in Figure 3, with total emissions in Figure S2 in Supporting Information S1 and population density in Figure S3 in Supporting Information S1. Note that the Los Angeles region within the observation domain has the largest population at approximately 4.3 million, while the Bay Area and Houston both have a population of approximately 3 million (3.0 and 3.1 million, respectively).

Both the Bay Area and Los Angeles regions show strong seasonality not present in the prior emissions. Houston shows a much weaker seasonal cycle. Comparison of the posterior to two independent activity-based inventories: the GReenhouse Gas And Air Pollutants Emissions System (GRA2PES) (Lyu et al., 2024) inventory for model year 2021 and the Carbon Monitor Cities (CMC) (Huo et al., 2022) inventory is shown in Figure S4 in Supporting Information S1 and summarized in Table S2 in Supporting Information S1. In each case, our posterior shares seasonality behavior with at least one other inventory.

The Bay Area posterior emissions demonstrate strong agreement with both GRA2PES and CMC, which indicate Bay Area emissions peak in winter. The Los Angeles posterior initially peaks before CMC's peak, but GRA2PES peaks concurrently with the posterior in Los Angeles. Additionally, the Los Angeles posterior exhibits a second peak coinciding with CMC's peak. The one-σ uncertainty range of the posterior typically encompasses both CMC and GRA2PES values in Los Angeles. Perfect alignment is not expected given different regional boundaries (Table S2 in Supporting Information S1).

In Houston, CMC predicts both summer and winter emission peaks, while GRA2PES predicts peak emissions in summer (Figure S4 in Supporting Information S1). Our posterior result supports the seasonality of the GRA2PES product, though the magnitude of posterior emissions (approximately 15 mol CO_2 h^{-1} $capita^{-1}$) is substantially lower than GRA2PES (>25 mol CO_2 h^{-1} $capita^{-1}$) and our Vulcan prior (approximately 20 mol CO_2 h^{-1} $capita^{-1}$). CMC is also higher than our posterior at approximately 20 mol CO_2 h^{-1} $capita^{-1}$. Notably, the CMC region for Houston includes a very large power plant (Figure S7 in Supporting Information S1), which is not included in the regions of the other inventories. COVID-19 activity changes may affect Houston's 2020 emissions. This effect would be captured in CMC, but not in GRA2PES (model year 2021). The substantial disagreement between GRA2PES and Vulcan for Houston highlights significant uncertainty in emissions estimates for this region. Our posterior provides an additional, observationally constrained estimate, but these results indicate a need for further study of the emissions in this region.

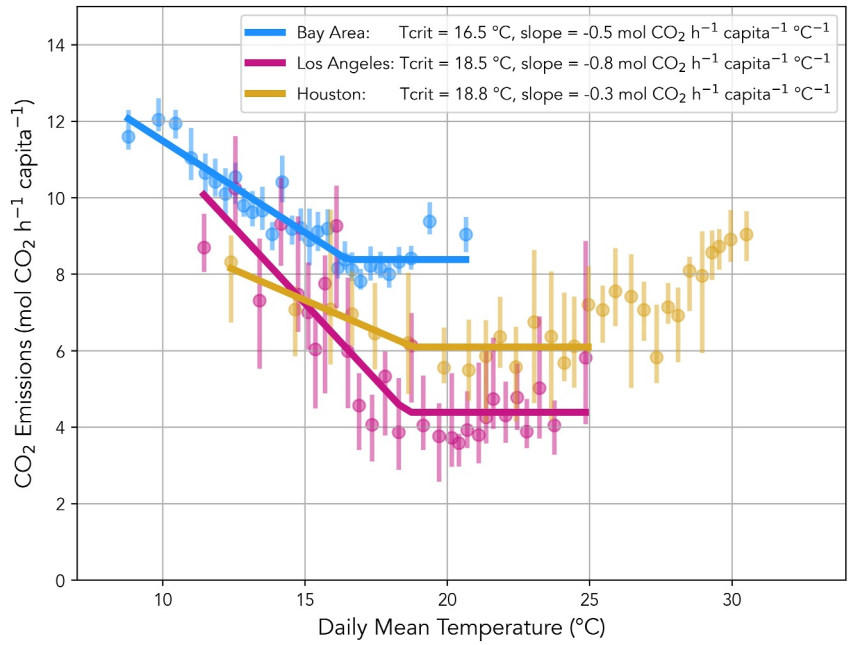

Figure 4. Emissions as a function of temperature. Daily mean temperatures and emissions from 0:00–6:00 local time were taken for each of the three regions, then sorted into 30 equally sized temperature bins. Error bars represent the 95% confidence interval in the median for each bin. A piecewise linear fitting is shown.

3.2. Impacts of Home Heating

The temperature dependence of the emissions is explored in Figure 4. Emissions follow the expected shape: flat at moderate temperatures with a linear increase below a critical temperature. At hot temperatures (particularly in Houston) we also obtain an increase in emissions, likely due to impacts of home cooling. For this analysis, the hottest temperatures (>25°C) are not analyzed and are left out of the fitting. We test the sensitivity of the derived T_{crit} to this assumption in Figure S12 in Supporting Information S1. After outlier removal and temperature binning (Section 2.5), a piecewise linear fitting allows us the determine the critical temperature and heating slope of each city. The fitting yields a T_{crit} of 16.5 ± 0.5°C ($R^2 = 0.87$) in the Bay Area, similar to the national median value of 16.5°C (Mittakola et al., 2024). In Los Angeles and Houston, we find T_{crit} of 18.5 ± 0.8°C ($R^2 = 0.73$) and 18.8 ± 1.2°C ($R^2 = 0.64$) respectively, slightly warmer than the national median. Having nearly 5 years of emissions posterior in the Bay Area, as opposed to 1 year in Houston or Los Angeles, gives a substantial decrease in uncertainty, as seen in the size of the confidence intervals for each temperature bin (Figure 4), the smaller in uncertainty on the T_{crit} value, and the higher R^2 value. Still, a remarkably clean relationship is also obvious in just 1 year of Los Angeles inversions. The poorer fitting (and corresponding larger uncertainty) in Houston results largely from the much smaller number of cold days than in Los Angeles during the study periods. A comparison of our derived T_{crit} values to those in Mittakola et al., 2024 is presented in Table S1 in Supporting Information S1, as well as the values obtained using solely monthly natural gas distribution data provided by the California gas utilities.

The slope of the emissions with regard to temperature for $T < T_{crit}$ provides an indication of the local carbon intensity of home heating in each city. We find that this slope is most strongly negative in Los Angeles (−0.8 ± 0.1 mol CO_2/h/capita/°C), and least strongly negative in Houston (−0.3 ± 0.1 mol CO_2/h/capita/°C). Bay Area values were in between (−0.5 ± 0.1 mol CO_2/h/capita/°C).

Emissions from electricity production play a larger role in Houston relative to the California cities (Figures S5 and S7 in Supporting Information S1), an effect which is apparent in both home heating and home cooling. In Houston, 61% of homes are heated with electricity, compared to 30% in the Bay Area and 32% in Los Angeles (Figure S6 in Supporting Information S1) (U.S. Census Bureau, 2023). Electric heating's carbon intensity varies with the local grid's fuel composition and often has lower efficiency than direct gas combustion. However, given that the BEACO$_2$N observing system is mostly sensitive to local emissions, and not all of the electricity used

within the region of influence is generated within the region of influence, we cannot draw conclusions on the carbon intensity of the heating systems from this analysis alone.

The effect of electricity production on home cooling is also apparent in Houston. Emissions increase dramatically at the warmest temperatures (Figure 4). Electricity demand in the region shows a similar trend at high temperatures to the posterior emissions (Figure S8 in Supporting Information S1). While power demand also shows some increases at lower temperatures (Figure S8 in Supporting Information S1), the corresponding rise in emissions is amplified by the contributions of natural gas heating.

In the Bay Area and Los Angeles, monthly posterior emissions have a moderately strong correlation with natural gas distribution data provided by the gas utility, though overall emissions tend to increase a month or so before reported natural gas distribution increases (Figure S9 in Supporting Information S1). Seasonality of other emission sectors as well as any potential biospheric fluxes not captured well by SIF could explain the differences in seasonality.

4. Conclusions

Home heating emissions are a significant contributor to urban CO_2 emissions and are strongly temperature dependent. Emissions from home heating (and cooling) are expected to change in coming decades due to both planetary warming and adoption of new heating and cooling technologies, such as electric heat pumps. Dense sensor networks combined with Bayesian inversions are promising methods for tracking these changes over time. Here we show that a dense CO_2 sensor network and Bayesian inversion system are sensitive to relatively small differences in regional home heating behavior.

Data Availability Statement

$BEACO_2N$ data is available at (BEACO2N, 2025). The STILT model is available at (Fasoli et al., n.d.). Inversion code is available at (Turner, 2020). OCO-2 GEOS L3 assimilated data set was received from the NASA Global Modeling and Assimilation Office (https://gmao.gsfc.nasa.gov/). SIF-GPP data is available at (Turner et al., 2022). Weather data is available from visualcrossing.com. The Vulcan v3 product is available from (Gurney et al., 2020). GRA2PES data is available at (Lyu et al., 2024). CMC data is available at https://cities.carbonmonitor.org/. PG&E data is available at https://pge-energydatarequest.com/. SoCalGas data is available at https://energydatarequest.socalgas.com/. ERCOT data is available from https://www.ercot.com/gridinfo/load/load_hist. ACS home heating fuel data is available from the U.S. Census Bureau (U.S. Census Bureau, 2023). Population density is available from (WorldPop & Bondarenko, 2020).

Acknowledgments
The authors thank Lesley Ott and Brad Weir at NASA Goddard for providing the OCO-2 GEOS 3D product used for prior background concentrations. We thank Rohith Teja for providing T_{crit} values for comparison. We acknowledge the support of all members of the $BEACO_2N$ Bay Area team: Alexis Shusterman, Virginia Teige, Kaitlyn Lieschke, Catherine Newman, Paul Wooldridge, Helen Fitzmaurice, Jinsol Kim, Erin Delaria, Kevin Worthington, and Pietro Vannucci for their work designing, calibrating, and maintaining the network. We acknowledge Nick Rollins for his work with the Carbon Census network. This material is based upon work supported by the National Science Foundation Graduate Research Fellowship Program under Grant 1752814. Any opinions, findings, and conclusions or recommendations expressed in this material are those of the author(s) and do not necessarily reflect the views of the National Science Foundation. The LA $BEACO_2N$ array (Carbon Census) was supported by USC Dornsife College and Public Exchange and a Presidents Fund Award to WB. This research used the Savio computational cluster resource provided by the Berkeley Research Computing program at the University of California, Berkeley (supported by the UC Berkeley Chancellor, Vice Chancellor for Research, and Chief Information Officer).

References

Alberini, A., Gans, W., & Velez-Lopez, D. (2011). Residential consumption of gas and electricity in the U.S.: The role of prices and income. *Energy Economics*, *33*(5), 870–881. https://doi.org/10.1016/j.eneco.2011.01.015

Asimow, N. G., Turner, A. J., & Cohen, R. C. (2024). Sustained reductions of Bay area CO_2 emissions 2018–2022. *Environmental Science and Technology*, *58*(15), 6586–6594. https://doi.org/10.1021/acs.est.3c09642

Baldocchi, D., & Penuelas, J. (2019). The physics and ecology of mining carbon dioxide from the atmosphere by ecosystems. *Global Change Biology*, *25*(4), 1191–1197. https://doi.org/10.1111/gcb.14559

BEACO2N. (2025). The Berkeley environmental air-quality and CO_2 network [Dataset]. *BEACO2N*. Retrieved from https://beacon.berkeley.edu/about/

Benjamin, S. G., Weygandt, S. S., Brown, J. M., Hu, M., Alexander, C. R., Smirnova, T. G., et al. (2016). A north American hourly assimilation and model forecast cycle: The rapid refresh. *Monthly Weather Review*, *144*(4), 1669–1694. https://doi.org/10.1175/MWR-D-15-0242.1

Brandt, A. R., Heath, G. A., Kort, E. A., O'Sullivan, F., Pétron, G., Jordaan, S. M., et al. (2014). Methane leaks from north American natural gas systems. *Science*, *343*(6172), 733–735. https://doi.org/10.1126/science.1247045

Breathe Providence. (n.d.). Breathe providence. Retrieved from https://www.breatheprovidence.com

Delaria, E. R., Kim, J., Fitzmaurice, H. L., Newman, C., Wooldridge, P. J., Worthington, K., & Cohen, R. C. (2021). The Berkeley environmental air-quality and CO_2 network: Field calibrations of sensor temperature dependence and assessment of network scale CO_2 accuracy. *Atmospheric Measurement Techniques*, *14*(8), 5487–5500. https://doi.org/10.5194/amt-14-5487-2021

EIA. (2017). Energy information administration (EIA)-about the residential energy consumption survey (RECS) table HC1.1 fuels used and end uses in U.S. Homes by housing unit type. Retrieved from https://www.eia.gov/consumption/residential/data/2015/hc/php/hc6.1.php

Fasoli, B., Lin, J. C., Bowling, D. R., Mitchell, L., & Mendoza, D. (2018). Simulating atmospheric tracer concentrations for spatially distributed receptors: Updates to the stochastic time-inverted Lagrangian transport model's R interface (STILT-R version 2). *Geoscientific Model Development*, *11*(7), 2813–2824. https://doi.org/10.5194/gmd-11-2813-2018

Fasoli, B., Mineau, J., & Lin, J. (n.d.). Stochastic time-inverted Lagrangian transport model [Computer software]. *STILT*. https://github.com/uataq/stilt

Feng, S., Lauvaux, T., Keller, K., Davis, K. J., Rayner, P., Oda, T., & Gurney, K. R. (2019). A road map for improving the treatment of uncertainties in high-resolution regional carbon flux inverse estimates. *Geophysical Research Letters*, *46*(22), 13461–13469. https://doi.org/10.1029/2019GL082987

GEMINOA. (n.d.). Geminoa. Retrieved from https://geminoa.strath.ai/about/

Gurney, K. R., Liang, J., Patarasuk, R., Song, Y., Huang, J., & Roest, G. (2020). *Vulcan: High-Resolution annual fossil fuel CO_2 emissions in USA, 2010–2015, version 3*. ORNL DAAC. https://doi.org/10.3334/ORNLDAAC/1741

Huo, D., Huang, X., Dou, X., Ciais, P., Li, Y., Deng, Z., et al. (2022). Carbon Monitor Cities near-real-time daily estimates of CO_2 emissions from 1500 cities worldwide. *Scientific Data*, *9*(1), 533. https://doi.org/10.1038/s41597-022-01657-z

IEA. (2021). Renewables 2021. Retrieved from https://www.iea.org/reports/renewables-2021

IPCC. (2006). IPCC guidelines for national greenhouse gas inventories. *Intergovernmental Panel on Climate Change*. Retrieved from https://www.ipcc-nggip.iges.or.jp/meeting/pdfiles/Washington_Report.pdf

IPCC. (2023a). Buildings. In *Climate change 2022—Mitigation of climate change: Working group III contribution to the sixth assessment report of the intergovernmental panel on climate change* (pp. 953–1048). Cambridge University Press. https://doi.org/10.1017/9781009157926.011

IPCC. (2023b). Synthesis report of the IPCC sixth assessment report (AR6). *IPCC*. Retrieved from https://www.ipcc.ch/report/ar6/syr/

IRS. (2023). SOI tax stats—Clean energy tax credit statistics. *Internal Revenue Service*. Retrieved from https://www.irs.gov/statistics/soi-tax-stats-clean-energy-tax-credit-statistics

Kim, J., Berelson, W. M., Rollins, N. E., Asimow, N. G., Newman, C., Cohen, R. C., et al. (2025). Observing anthropogenic and biogenic CO_2 emissions in Los Angeles using a dense sensor network. *Environmental Science and Technology*, *59*(7), 3508–3517. https://doi.org/10.1021/acs.est.4c11392

Lian, J., Lauvaux, T., Utard, H., Bréon, F.-M., Broquet, G., Ramonet, M., et al. (2023). Can we use atmospheric CO_2 measurements to verify emission trends reported by cities? Lessons from a 6-year atmospheric inversion over Paris. *Atmospheric Chemistry and Physics*, *23*(15), 8823–8835. https://doi.org/10.5194/acp-23-8823-2023

Lin, J. C., Gerbig, C., Wofsy, S. C., Andrews, A. E., Daube, B. C., Davis, K. J., & Grainger, C. A. (2003). A near-field tool for simulating the upstream influence of atmospheric observations: The Stochastic Time-Inverted Lagrangian Transport (STILT) model. *Journal of Geophysical Research*, *108*(D16), 4493. https://doi.org/10.1029/2002JD003161

Lyu, C., Harkins, C., Li, M., McDonald, B., Prothero, J., & Mueller, K. (2024). *The U.S. Greenhouse gas and air pollutant emissions system (GRA2PES) (version 1.0.0, p. 230 files, 1.53 TB) [Application/gzip,application/pdf,application/x-netcdf]*. National Institute of Standards and Technology. https://doi.org/10.18434/MDS2-3520

Mangat, T. S., Claire, S. J., Dinh, T. M., Fanai, A. K., Nguyen, M. H., & Schultz, S. A. (2010). Source inventory of Bay area greenhouse gas emissions. *Bay Area Air Quality Management District*.

Martin, C. R., Zeng, N., Karion, A., Mueller, K., Ghosh, S., Lopez-Coto, I., et al. (2019). Investigating sources of variability and error in simulations of carbon dioxide in an urban region. *Atmospheric Environment*, *199*, 55–69. https://doi.org/10.1016/j.atmosenv.2018.11.013

McDonald, B. C., McBride, Z. C., Martin, E. W., & Harley, R. A. (2014). High-resolution mapping of motor vehicle carbon dioxide emissions. *Journal of Geophysical Research: Atmospheres*, *119*(9), 5283–5298. https://doi.org/10.1002/2013JD021219

Mittakola, R. T., Ciais, P., Schubert, J. E., Makowski, D., Zhou, C., Bazzi, H., et al. (2024). Drivers of natural gas use in U.S. residential buildings. *Science Advances*, *10*(14), eadh5543. https://doi.org/10.1126/sciadv.adh5543

Munassar, S., Monteil, G., Scholze, M., Karstens, U., Rödenbeck, C., Koch, F.-T., et al. (2023). Why do inverse models disagree? A case study with two European CO_2 inversions. *Atmospheric Chemistry and Physics*, *23*(4), 2813–2828. https://doi.org/10.5194/acp-23-2813-2023

Newville, M., Otten, R., Nelson, A., Stensitzki, T., Ingargiola, A., Allan, D., et al. (2024). lmfit/lmfit-py: 1.3.2 (Version 1.3.2) [Computer software]. *Zenodo*. https://doi.org/10.5281/zenodo.12785036

Palecki, M., Durre, I., Applequist, S., Arguez, A., & Lawrimore, J. (2020). U.S. Climate normals 2020: U.S. Hourly climate normals (1991–2020) [Dataset]. *NOAA National Centers for Environmental Information*. https://www.ncei.noaa.gov/metadata/geoportal/rest/metadata/item/gov.noaa.ncdc:C01619/html

Shusterman, A. A., Teige, V. E., Turner, A. J., Newman, C., Kim, J., & Cohen, R. C. (2016). The Berkeley atmospheric CO_2 observation network: Initial evaluation. *Atmospheric Chemistry and Physics*, *16*(21), 13449–13463. https://doi.org/10.5194/acp-16-13449-2016

Turner, A. J. (2020). UrbanInversion [Computer software]. https://github.com/alexjturner/UrbanInversion

Turner, A. J., Kim, J., Fitzmaurice, H., Newman, C., Worthington, K., Chan, K., et al. (2020). Observed impacts of COVID-19 on urban CO_2 emissions. *Geophysical Research Letters*, *47*(22), e2020GL090037. https://doi.org/10.1029/2020GL090037

Turner, A. J., Koehler, P., Magney, T., Frankenberg, C., Fung, I., & Cohen, R. C. (2022). *Carbon monitoring system (CMS) CMS: Daily Gross primary productivity over CONUS from TROPOMI SIF, 2018-2021 (version 1, p. 0 MB) [netCDF]*. ORNL Distributed Active Archive Center. https://doi.org/10.3334/ORNLDAAC/1875

Turner, A. J., Köhler, P., Magney, T. S., Frankenberg, C., Fung, I., & Cohen, R. C. (2021). Extreme events driving year-to-year differences in gross primary productivity across the US. *Biogeosciences*, *18*(24), 6579–6588. https://doi.org/10.5194/bg-18-6579-2021

Turner, A. J., Shusterman, A. A., McDonald, B. C., Teige, V., Harley, R. A., & Cohen, R. C. (2016). Network design for quantifying urban CO_2 emissions: Assessing trade-offs between precision and network density. *Atmospheric Chemistry and Physics*, *16*(21), 13465–13475. https://doi.org/10.5194/acp-16-13465-2016

U.S. Census Bureau. (2023). House heating fuel," 2023 American community Survey 1-year estimates subject Tables, table B25040 [Dataset]. *U.S. Census Bureau*. Retrieved from https://data.census.gov/table/ACSDT1Y2023.B25040?q=B25040:%20House%20Heating%20Fuel

Verhallen, T. M. M., & van Raaij, W. F. (1981). Household behavior and the use of natural gas for home heating. *Journal of Consumer Research*, *8*(3), 253–257. https://doi.org/10.1086/208862

Visual Crossing. (n.d.). Weather data and weather API | visual crossing. Retrieved from https://www.visualcrossing.com/

Walker, I. S., Less, B. D., & Casquero-Modrego, N. (2022). Carbon and energy cost impacts of electrification of space heating with heat pumps in the US. *Energy and Buildings*, *259*, 111910. https://doi.org/10.1016/j.enbuild.2022.111910

Weir, B., Crisp, D., O'Dell, C. W., Basu, S., Chatterjee, A., Kolassa, J., et al. (2021). Regional impacts of COVID-19 on carbon dioxide detected worldwide from space. *Science Advances*, *7*(45), eabf9415. https://doi.org/10.1126/sciadv.abf9415

Winter, A. R., Zhu, Y., Asimow, N. G., Patel, M. Y., & Cohen, R. C. (2025). A scalable calibration method for enhanced accuracy in dense air quality monitoring networks. *Environmental Science and Technology*, *59*(5), 2599–2610. https://doi.org/10.1021/acs.est.4c08855

WorldPop, & Bondarenko, M. (2020). Individual countries 1 km population density (2000-2020) [Dataset]. *University of Southampton*. https://doi.org/10.5258/SOTON/WP00674

Yadav, V., & Michalak, A. M. (2013). Improving computational efficiency in large linear inverse problems: An example from carbon dioxide flux estimation. *Geoscientific Model Development*, *6*(3), 583–590. https://doi.org/10.5194/gmd-6-583-2013

Yang, Y., Zhao, M., Xu, X., Sun, Z., Yin, G., & Piao, S. (2014). Diurnal and seasonal change in stem respiration of larix principis-rupprechtii trees, northern China. *PLoS One*, *9*(2), e89294. https://doi.org/10.1371/journal.pone.0089294

References From the Supporting Information

EIA. (2022). *Electricity generation, capacity, and sales in the United States—Top 10*. U.S. Energy Information Administration (EIA). Retrieved from https://www.eia.gov/energyexplained/electricity/electricity-in-the-us-top-10.php

EPA. (n.d.). GHG facility details. Retrieved from https://ghgdata.epa.gov/ghgp/service/facilityDetail/2020?id=1006868&ds=E&et=&popup=true

ERCOT. (n.d.). Hourly load data archives. *ERCOT*. Retrieved from https://www.ercot.com/gridinfo/load/load_hist

Google Maps. (n.d.). W. A. Parish generating station · 2500 Y. U. Jones Rd, Richmond, TX 77469. Retrieved from https://www.google.com/maps/place/W.A.+Parish+Generating+Station/data=!4m2!3m1!1s0x0:0x2863691d12367c50?sa=X&ved=1t:2428&ictx=111

PG&E. (n.d.). PG&E's energy data request portal. *PG&E*. Retrieved from https://pge-energydatarequest.com/public_datasets

SoCalGas. (n.d.). Energy data request program. *SoCalGas*. Retrieved from https://energydatarequest.socalgas.com/